Astron. Astrophys. 327, 602–613 (1997)

ASTRONOMY AND ASTROPHYSICS

Cataclysmic variables in the ROSAT PSPC All Sky Survey

F. Verbunt[1,2], **W.H. Bunk**[2], **H. Ritter**[3], **and E. Pfeffermann**[2]

[1] Astronomical Institute, P.O.Box 80000, 3508 TA Utrecht, The Netherlands
[2] Max Planck Institut für extraterrestrische Physik, D-85740 Garching bei München, Germany
[3] Max Planck Institut für Astrophysik, D-85740 Garching bei München, Germany

Received 20 February 1997 / Accepted 29 April 1997

Abstract. 91 cataclysmic variables from a sample of 162 systems with known or suspected binary periods were detected during the ROSAT XRT-PSPC All Sky Survey. Among the non-magnetic systems, the X-ray to optical/ultraviolet flux ratio decreases along the sequence SU UMa type – U Gem type – Z Cam type – UX UMa type, due mainly to variations in the optical/ultraviolet flux. 8 of the 10 brightest systems in terms of total PSPC countrate are magnetic systems. The 0.5-2.5 keV X-ray luminosities range up to $\sim 10^{32}$erg/s, the highest luminosities being those of four faraway DQ Her type systems. The other types of cataclysmic variables all have similar 0.5-2.5 keV luminosity distributions. In an Appendix we compare the X-ray properties of cataclysmic variables with those of the dim X-ray sources in globular clusters.

Key words: cataclysmic variables – globular clusters – X-rays: stars

1. Introduction

It was recognized in the 1950s that the various phenomena displayed by the cataclysmic variables, including nova outbursts, dwarf-nova outbursts, and nova-like variability, are all the consequence of accretion onto a white dwarf of matter from a low-mass donor star (see, e.g., Kraft 1990, Warner 1976, 1995). More than 550 cataclysmic variables are now known, many of them discovered through optical observations, and some, especially those in which the white dwarf has a strong magnetic field, discovered first through X-ray observations. Those with known or suspected orbital period are listed by Ritter & Kolb (1995).

Cataclysmic variables are in general not very bright in X-rays. The first one detected in X-rays, with rocket experiments, was the dwarf nova SS Cyg (Rappaport et al. 1974; see also Heise et al. 1978). The UHURU satellite detected just two cataclysmic variables, neither of them immediately recognized as such: Warner (1976) proposed the identification of 4U1249−28 with EX Hya, and the variable AM Her turned out on further optical study to be a cataclysmic variable (Forman et al. 1978). Both of these cataclysmic variables contain a white dwarf with a strong magnetic field. A few dozens of cataclysmic variables have been detected since in X-rays with the HEAO-1 satellite, with EXOSAT, and especially with the Einstein satellite, as reviewed by e.g. Córdova & Mason (1983) and by Córdova (1995). A reanalysis of the Einstein data has been made by Eracleous et al. (1991; see also Patterson & Raymond 1985).

Our knowledge of the X-ray emission of cataclysmic variables is still very limited with respect to the location in the binary of the X-ray emission, to the spectral flux distribution, and to the total X-ray luminosity. Observations with recent, highly sensitive satellites such as ROSAT, ASCA and EUVE, are transforming the field (for reviews, see, e.g. Mauche 1997, Verbunt 1996b).

In this paper we present the data from the ROSAT PSPC All Sky Survey on cataclysmic variables. We limit ourselves to such systems that were known to be cataclysmic variables before ROSAT was launched, and whose orbital period was known, collected in the catalogue by Ritter (1990). The observations and data reduction are described in Sect. 2, the results in Sect. 3. A discussion follows in Sect. 4.

Some results from the ROSAT PSPC All Sky Survey have been presented before by Beuermann & Thomas (1993) for the total sample of cataclysmic variables, and by Wheatley et al. (1996b), Ponman et al. (1995) and Wheatley et al. (1996a) on the individual systems VW Hyi, SS Cyg and Z Cam, respectively. New cataclysmic variables discovered from the optical identification of X-ray sources from the ROSAT PSPC All Sky Survey are described by e.g. Motch et al. (1996).

The nomenclature of cataclysmic variables is not well established, and therefore we briefly describe the classification that we use in this paper. The cataclysmic variables that show optical outbursts during which the optical flux is increased by a factor $\lesssim 100$ during a few days are called *dwarf novae*. The outbursts are irregularly spaced, with average intervals ranging from $\gtrsim 1$ week in some systems to 30 yr in others. Dwarf novae whose outbursts are occasionally interspersed with stronger and longer outbursts (the 'superoutbursts') are the *SU UMa* systems. Dwarf

Send offprint requests to: F. Verbunt, Utrecht

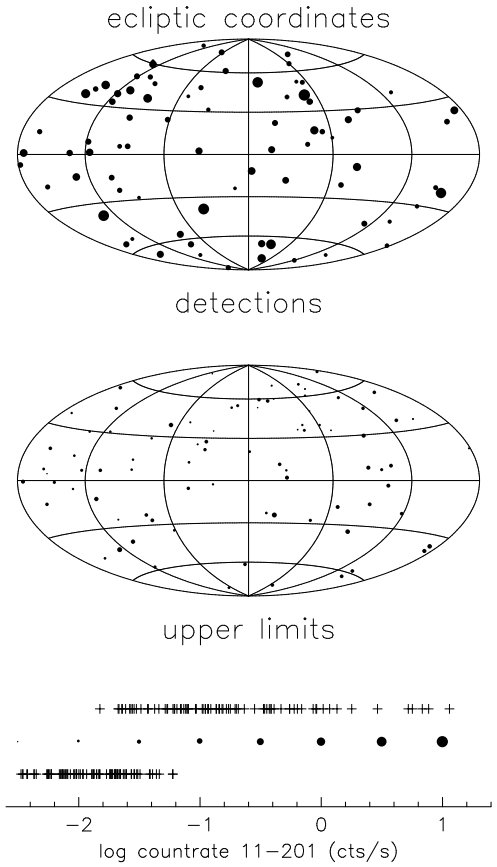

Fig. 1. The position in the sky, in ecliptic coordinates, of the sources detected in channels 11-201 (top) and of the sources for which only an upper limit was obtained (middle). The ecliptic is the central horizontal line, which runs from 180° left to −180° right. The size of the symbols is proportional to the logarithm of the countrate, as indicated in the lowest panel, where we also show the distributions in countrate of the detections (above) and upper limits (below).

novae in which the decline to quiescence is sometimes halted for a period of several weeks during which the systems lingers at a flux level well above quiescence (the 'standstill') are the *Z Cam* systems. The remaining dwarf novae are the *U Gem* systems. The cataclysmic variables that do not show outbursts we will refer to as the *nova-like variables*. Those in which a strong magnetic field locks the white-dwarf rotation to the binary revolution are the *AM Her* systems or polars. Nova-like variables whose white dwarfs have strong magnetic fields, enough to disrupt the inner disk but not to lock the white dwarf to the orbit, are the *DQ Her* systems or intermediate polars. (Whether locking occurs depends on the field strength and on the size of the orbit, thus on the orbital period.) Those in which no evidence has been found for a magnetic field of the white dwarf we will refer to as the *UX UMa* systems.

Cataclysmic variables that are known to have undergone a nova outburst, the old novae, are included in the above classes; we show them separately in diagrams. Finally, those cataclysmic variables, like AM CVn, in which the mass donor is also a white dwarf are the *double degenerate* systems.

2. Observations and data reduction

Between July 1990 and January 1991 a survey of the whole sky was made with the ROSAT X-ray telescope and position-sensitive proportional counter (PSPC). Some areas of the sky missed during this period were added in February and August 1991. The instrumentation is described by Pfeffermann et al. (1986), and the Survey by Voges (1992). During the Survey, the ROSAT satellite scanned a great circle of the sky during each revolution of about 90 minutes. With a field of view of about 2 degrees, the X-ray detector observed a source passing through the center for about 30 seconds. The precession of the satellite orbit caused the position of the scan to shift slowly, so that the whole sky was observed in half a year. The observations of a source with ecliptical longitude and latitude λ,β are roughly centered on[1]

$$\mathrm{JD} \simeq 2448051.6 + 1.052[(\lambda - 50) \bmod 180] \quad (1)$$

and have a separation between the first and last scan of roughly $2/\cos\beta$ days. The actual obtained exposure is often much shorter than the geometric exposure time during which the source is scanned, due to occultation of the source by the PSPC window support structure, and to interruption of observations near very bright sources and as the satellite passes through the South Atlantic Anomaly. A few cataclysmic variables are in parts of the sky which were observed some time after the nominal survey period; these are indicated in Tables 1,2. Four systems are in areas of the sky observed less than 50 s; these systems, CP Eri, UZ For, U Sco and EXO 0329 − 26, are omitted from the analysis. The survey data were analyzed with the EXSAS software (Zimmermann et al. 1992), as follows. In a first analysis, we use energy channels 11-201 of the PSPC, corresponding roughly to photon energies between 0.1 and 2.0 keV. We use a sliding-box algorithm to detect sources, using a local estimate of the background, in a field of $1^\circ \times 1^\circ$, centered on the cataclysmic variable. The algorithm localizes sources, and provides a maximum-likelyhood parameter L which corresponds to a probability of $\exp(-L)$ for a single trial that the source is a chance enhancement over the background. The sources with $L > 7$ are retained, their positions determined, and then all counts in a circle with a radius of $5'$ around each position are subtracted from the image. A bicubic spline fit is made to the remaining background. We then return to the full data set, and at each position within a circle with $5'$ radius around the position of the cataclysmic variable (taken from the catalogue of Ritter 1990), use this bicubic spline fit in the determination of the excess countrate above background, with the maximum likelihood algorithm described by Cruddace et al. (1988), which treats each photon individually and determines the best source position. The result of this calculation was considered a detection if $L > 10$,

[1] the equation given in Verbunt et al. 1995 is wrong

Table 1. Cataclysmic variables detections in the ROSAT All Sky Survey. The first two columns give the name of the system and its type: 1 dwarf nova of unspecified type, 2 SU UMa system, 3 Z Cam system, 4 U Gem system, 5 AM Her system, 6 DQ Her system, 7 UX UMa system, 8 double degenerate, 9 old nova, 0 unclassified. The type-indicator is followed by a 1 in the third column if the system was detected first because of its X-ray emission. The total number of counts detected, and the effective exposure time (i.e. corrected for reduced off–axis sensitivity) are in columns 4 and 5. The ratio of these two numbers gives the total countrate. The remaining columns give the counts detected in channel ranges A (channels 11-41), B (52-201), C (52-90) and D (91-201), not corrected for vignetting, the countrate in range B (cts/s), the visual magnitude, the adopted distance, and the X-ray luminosity in the 0.5-2.5 keV band (not corrected for interstellar absorption). The visual magnitude is the magnitude at which the system is most frequently found, MAG1 in Ritter (1990); the actual magnitude during the Survey may be different. Sources for the distances are: Warner 1987, Rutten et al. 1992 and Sproats et al. 1996 for dwarf novae and non-magnetic systems, Tables 6.1 and 7.4 in Warner 1995 for magnetic systems, and Reimers et al. 1988 for CQ Dra BC.

name	T	X	cts 11-201	t_{exp}(s)	cts 11-41	cts 52-201	cts 52-90	cts 91-201	log ctr 52-201	V	d(pc)	log L_x (erg/s)
FO And	4	0	0(9)	377.4	0(4)	8(3)	0(7)	0(5)	−1.70	17.5		
RX And	3	0	15(5)	414.2	0(5)	14(4)	0(10)	9(3)	−1.46	12.6	135	30.0
UU Aql	2	0	8(4)	370.7	0(4)	7(3)	0(3)	5(3)	−1.71	16.1	225	30.2
V603 Aql	9	0	131(12)	350.8	12(4)	118(11)	54(8)	64(8)	−0.48	11.4		
V794 Aql	7	0	36(7)	382.1	0(2)	37(7)	12(4)	25(5)	−1.02	13.7		
AE Aqr	6	0	365(20)	403.2	188(14)	167(13)	70(9)	97(10)	−0.38	10.9	140	31.1
VY Aqr	4	0	28(7)	434.2	0(11)	18(5)	0(6)	15(4)	−1.38	17.1	97	29.8
TT Ari	7	0	115(11)	298.0	12(4)	102(11)	33(6)	70(9)	−0.46	9.5	185	31.3
FS Aur	2	0	50(8)	453.1	0(2)	52(8)	16(4)	36(6)	−0.94	16.2		
KR Aur	7	0	20(5)	375.3	0(4)	21(5)	0(5)	18(5)	−1.26	11.3		
SS Aur	2	0	69(9)	354.5	0(6)	65(9)	16(4)	49(7)	−0.74	14.5	200	31.1
CR Boo	8	0	36(7)	308.5	24(6)	11(4)	0(8)	0(8)	−1.45	13.0		
BY Cam	5	1	526(23)	390.2	286(17)	213(15)	62(8)	151(13)	−0.26	14.6	190	31.5
BZ Cam	7	0	28(6)	448.0	0(4)	31(6)	13(4)	18(5)	−1.16			
Z Cam	3	0	39(8)	491.1	19(5)	24(6)	11(4)	13(4)	−1.31	13.6	175	30.4
OY Car	4	0	15(5)	620.5	0(3)	15(5)	0(4)	12(4)	−1.63	15.3	100	29.6
HT Cas[a]	4	0	31(7)	406.0	0(16)	25(6)	0(9)	20(5)	−1.21	16.4	165	30.4
BV Cen[a]	2	0	5(3)	156.4	0(3)	0(4)	0(4)	0(6)		12.6		
V803 Cen	8	0	12(4)	293.5	0(2)	12(4)	0(6)	8(3)	−1.38	13.2		
WW Cet	3	0	221(16)	368.9	39(7)	175(14)	63(8)	112(11)	−0.32	15.0	100	30.9
WX Cet	1	0	10(4)	477.6	0(5)	0(6)	0(2)	0(4)		17.5	185	
Z Cha	4	0	31(7)	590.5	0(6)	28(6)	8(3)	21(5)	−1.33	15.3	130	30.1
SY Cnc	3	0	61(9)	305.9	18(5)	45(7)	19(5)	26(5)	−0.83	13.5		
YZ Cnc	4	0	69(9)	448.7	28(6)	44(7)	15(4)	30(6)	−1.01	14.1	290	31.1
TV Col	6	1	174(15)	511.3	31(7)	144(13)	47(7)	99(10)	−0.55	13.6	500	32.0
TX Col	6	1	119(12)	667.6	30(7)	86(10)	25(5)	61(8)	−0.89	15.7	550	31.8
GP Com	8	0	183(14)	266.0	82(10)	97(10)	39(7)	58(8)	−0.44	15.7		
EM Cyg	3	0	34(7)	567.7	0(4)	35(7)	0(7)	28(6)	−1.21	13.3	350	31.1
EY Cyg	2	0	15(5)	585.0	0(3)	16(5)	7(3)	9(4)	−1.55	15.5		
SS Cyg	2	0	4131(67)	733.0	3361(58)	693(27)	319(18)	375(20)	−0.02	11.4	75	30.9
V1500 Cyg	5	0	0(16)	844.4	0(5)	12(5)	0(8)	0(6)	−1.83	17.1	1200	31.5
AB Dra	3	0	156(14)	1145.7	0(11)	153(13)	47(7)	107(11)	−0.88	14.5		
CQ Dra BC	0	0	11(5)	716.0	0(5)	16(5)	0(3)	17(5)	−1.66		100	29.5
DM Dra	2	0	0(15)	1102.3	0(6)	0(9)	8(3)	0(2)		21.7	580	
DO Dra	1	1	438(23)	799.0	180(15)	251(17)	97(10)	155(13)	−0.50			
EF Eri	5	1	1614(41)	210.1	1301(36)	284(17)	118(11)	169(13)	0.13	13.7	94	31.3
IR Gem	4	0	56(8)	451.9	20(5)	34(6)	14(4)	20(5)	−1.12	16.3		
U Gem	2	0	157(13)	337.2	51(8)	105(11)	29(6)	76(9)	−0.51	14.0	81	30.5
AH Her	3	0	0(10)	547.8	0(5)	8(3)	0(4)	6(3)	−1.86	13.9	250	30.1
AM Her	5	0	181(15)	1561.7	82(10)	99(11)	39(7)	60(8)	−1.20	12.0	75	29.8
V795 Her	7	0	0(11)	770.5	0(5)	9(4)	0(6)	6(3)	−1.91			
EX Hya	6	0	1640(41)	314.3	586(25)	1001(32)	375(20)	628(25)	0.50	13.0	105	31.7
BL Hyi	5	1	766(28)	263.3	703(27)	57(8)	25(5)	32(6)	−0.67	14.3	128	30.7
VW Hyi	4	0	567(25)	547.2	268(17)	279(17)	112(11)	167(13)	−0.29	13.4	65	30.5
WX Hyi	4	0	277(18)	677.7	78(10)	202(15)	72(9)	131(12)	−0.53	14.7	265	31.5
DP Leo	5	1	33(7)	427.3	32(7)	0(5)	0(5)	0(2)			450	
T Leo	4	0	277(18)	436.5	105(11)	162(13)	74(9)	88(10)	−0.43	15.2	76	30.5

Table 1. (continued)

name	T	X	cts 11-201	$t_{\rm exp}$(s)	cts 11-41	cts 52-201	cts 52-90	cts 91-201	log ctr 52-201	V	d(pc)	log $L_{\rm x}$ (erg/s)
AY Lyr	4	0	0(7)	919.4	0(4)	7(3)	0(6)	0(3)	−2.14		52	28.5
MV Lyr	7	0	61(9)	869.6	0(8)	60(9)	10(4)	53(8)	−1.16	12.1	322	31.1
CW Mon	2	0	40(7)	493.0	0(2)	46(7)	12(4)	34(6)	−1.03	16.3	290	31.1
GQ Mus[a]	9	0	0(3)	122.0	0(8)	0(5)	5(2)	0(2)		17.5	290	
V426 Oph	3	0	59(9)	390.6	0(4)	63(9)	13(4)	52(8)	−0.80	11.5	100	30.4
V841 Oph	9	0	0(10)	402.5	0(3)	0(7)	0(5)	7(3)		13.5	255	
CN Ori	3	0	11(4)	517.3	0(3)	11(4)	5(3)	7(3)	−1.66	14.2	295	30.5
V1193 Ori	7	0	0(9)	440.0	0(9)	12(4)	0(5)	12(4)	−1.57	14.1		
BD Pav	2	0	0(6)	138.6	0(2)	9(3)	0(5)	6(3)	−1.20	15.4		
RU Peg	2	0	40(7)	280.2	9(3)	32(6)	22(5)	10(3)	−0.95	12.7	174	30.7
GK Per	6	0	54(8)	490.1	0(7)	56(8)	14(4)	43(7)	−0.94	10.2	340	31.3
UV Per	4	0	14(5)	611.4	0(3)	13(4)	0(5)	10(3)	−1.67	17.5	115	29.7
RR Pic	9	0	97(12)	1315.7	77(10)	16(5)	0(9)	0(9)	−1.92	12.0		
TY PsA	4	0	52(8)	182.9	18(5)	33(6)	13(4)	20(5)	−0.75	16.0		
AO Psc	6	1	112(11)	336.5	13(4)	97(10)	23(5)	75(9)	−0.54	13.3	420	31.9
BV Pup	2	0	0(14)	232.4	0(2)	14(4)	0(6)	10(3)	−1.23	15.0		
CP Pup	9	0	14(5)	520.4	0(5)	16(5)	0(6)	10(4)	−1.51	15.0		
VV Pup	5	0	2427(50)	356.7	2372(49)	20(5)	10(4)	12(4)	−1.25	14.5	145	30.3
V347 Pup	7	0	34(8)	1178.0	23(6)	12(5)	0(7)	0(10)	−1.99	13.4		
VY Scl	7	0	0(5)	82.3	0(2)	0(4)	4(2)	0(2)		12.9		
MR Ser	5	0	18(6)	588.9	0(6)	13(4)	0(7)	8(3)	−1.67	14.9	139	29.8
RW Sex	7	0	30(6)	431.9	0(8)	25(6)	11(4)	15(4)	−1.23	10.4		
RZ Sge	4	0	11(4)	390.0	0(2)	12(4)	0(7)	8(3)	−1.51	16.9		
WZ Sge	4	0	104(11)	503.4	45(8)	54(8)	21(5)	33(6)	−0.97	14.9		
V1223 Sgr	6	1	233(16)	271.6	42(7)	181(14)	60(8)	123(11)	−0.18	12.3	600	32.6
V3885 Sgr	7	0	32(7)	304.7	15(5)	17(5)	9(4)	9(3)	−1.25	9.6		
EK TrA	4	0	19(5)	136.0	0(5)	17(4)	0(4)	14(4)	−0.91	>17.0		
AN UMa	5	0	808(29)	453.7	787(29)	17(5)	8(3)	9(4)	−1.43	14.5	270	30.6
BZ UMa	1	0	162(14)	419.5	78(10)	84(10)	31(6)	53(8)	−0.70	17.8		
CH UMa	2	0	69(9)	478.6	0(7)	66(8)	30(6)	36(6)	−0.86	15.9		
CY UMa	4	0	49(8)	531.4	23(6)	24(5)	6(3)	19(5)	−1.34	17.0		
EI UMa	2	0	275(17)	501.4	91(10)	173(14)	64(8)	105(10)	−0.46			
EK UMa	5	1	699(28)	597.1	685(27)	0(4)	0(7)	0(2)		18.0		
SU UMa	4	0	381(20)	415.9	154(13)	218(15)	75(9)	143(12)	−0.28	14.2	280	31.8
SW UMa	4	0	81(10)	351.1	42(7)	36(6)	14(4)	22(5)	−0.99	16.5	140	30.5
SS UMi	2	0	49(9)	1308.7	0(9)	52(8)	21(5)	31(6)	−1.40	16.9		
CU Vel	4	0	93(11)	563.9	38(7)	54(8)	18(5)	36(7)	−1.02	15.5		
IX Vel	7	0	252(17)	707.9	131(13)	115(11)	49(7)	65(9)	−0.79	9.1	150	30.8
KO Vel	6	1	16(5)	353.5	0(6)	13(4)	0(9)	7(3)	−1.42	16.7		
TW Vir	2	0	39(7)	369.0	11(4)	27(6)	9(3)	19(5)	−1.13	15.8	455	31.4
QQ Vul	5	1	6002(96)	526.5	5839(93)	55(8)	29(6)	27(6)	−0.98	14.5	320	31.2
VW Vul	1	0	31(7)	582.1	0(4)	31(6)	6(3)	26(6)	−1.28	13.6		
GD552	0	0	113(12)	657.3	65(9)	47(8)	20(5)	27(6)	−1.15	16.5		
1329-294	1	0	18(5)	285.3	0(4)	16(5)	0(7)	9(3)	−1.25	17.4		

[a] observed in period 5-10 August 1991

and an upper limit otherwise. Of 162 sources investigated, 79 were detected in the analysis of channels 11-201.

Because the background is higher at energies less than 0.5 keV, faint sources may be detected more efficiently if the analysis is limited to higher energies. We have repeated the analysis described above for four separate bandpasses: A (channels 11-41), B (channels 52-201), C (channels 52-90) and D (channels 91-201). This resulted in the detection of eight more sources in band B. Three sources, DM Dra, GQ Mus and VY Scl were detected only in band C, and one source, V841 Oph, only in band D. In addition, the two sources BV Cen and WX Cet were not detected in any separate band; the detections of these two sources must be considered marginal. Two sources, DP Leo and EK UMa, were not detected in any of the hard bands B, C or D; both are *AM Her* systems, and were detected in the total band as well as in the A band. The ecliptic coordinates of the detected sources and of the upper limits are shown in Fig. 1.

Table 2. Cataclysmic variables not detected in the ROSAT All Sky Survey. The first three columns are as in Table 1, and are followed by 2-σ upper limits to the counts detected in the total channel range and in B (channels 50-201), the effective exposure time, the visual magnitude (MAG1 in Ritter 1990), and the distance. The count limits are not corrected for vignetting.

name	T	X		'B'	t_{exp}	V	d(pc)	name	T	X		'B'	t_{exp}	V	d(pc)
AR And	2	0	2	2	369.1	16.9	269	DI Lac	9	0	4	2	298.7	14.3	
HV And	7	0	2	2	536.2			DO Leo	1	0	4	5	380.6		878
V1315 Aql	7	0	2	4	515.0	14.4	300	RZ Leo	1	0	13	8	433.3	19.0	174
FO Aqr	6	1	9	4	314.9	13.0	325	U Leo	9	0	2	2	694.3	17.3	
HL Aqr	7	0	4	4	204.4	13.5		X Leo	2	0	6	3	404.5	15.8	
UU Aqr	7	0	2	3	282.4	13.5		ST LMi	5	0	4	5	215.9	15.0	128
WX Ari[a]	7	0	3	7	159.1	15.3	198	BR Lup	4	0	9	3	419.9	>17.5	
T Aur	9	0	4	4	457.0	14.9		BH Lyn	7	0	4	2	487.6	14.5	
V363 Aur	7	0	4	4	461.9	14.2	600	TU Men	4	0	11	7	529.7	>16.0	270
TT Boo	4	0	10	7	509.5	>15.6		BT Mon	9	0	3	3	495.6	15.4	
UZ Boo	1	0	3	3	534.4			V380 Oph	0	0	13	6	414.0	14.5	
AF Cam	1	0	9	7	223.9	17.0	425	V442 Oph	7	0	5	2	342.8	14.0	
QU Car	7	0	11	4	489.9	11.1		V2051 Oph	1	0	9	8	326.9	15.0	
V425 Cas	7	0	4	3	440.4	14.5		IP Peg	2	0	5	6	459.1	14.0	124
V436 Cen	4	0	10	7	302.7	15.3	210	FY Per	7	0	4	4	504.8	11.2	
V442 Cen	2	0	3	2	75.5	>16.5		V Per	9	0	3	3	570.4	18.5	
HL CMa	3	1	12	4	303.8	13.2	210	TW Pic	6	1	8	4	698.3	14.3	
BG CMi	6	1	16	7	428.4	14.3	700	AY Psc	7	0	3	2	433.4	14.9	565
AC Cnc	7	0	3	3	353.1	13.8	800	TY Psc	4	0	6	4	371.9	15.3	
AR Cnc	1	0	4	3	377.5	>17.4	681	V348 Pup	0	1	7	3	503.9	15.0	
AT Cnc	3	0	3	3	227.0			T Pyx	9	0	5	4	511.1	15.3	
AL Com	1	0	2	3	426.1	12.8	190	VZ Scl	7	0	3	2	323.1	15.6	530
V394 CrA	9	0	3	3	137.5	20.0		LX Ser[a]	7	0	8	3	362.3	14.5	340
AM CVn	8	0	4	2	531.8	14.1		UZ Ser	2	0	10	3	315.7	15.5	300
V503 Cyg	4	0	4	5	862.0	17.4		SW Sex	7	0	7	5	378.7		450
V751 Cyg	7	0	14	6	683.3	13.2		V Sge	7	0	4	4	507.9	12.2	
V1668 Cyg	9	0	3	3	721.6	20.0		WY Sge	9	0	4	6	549.4		
CM Del	2	0	6	2	482.3	13.4	280	V4140 Sgr	1	0	9	11	324.7	17.5	
HR Del	9	0	2	2	538.1	11.9	285	RW Tri[a]	7	0	3	2	262.6	12.6	270
AH Eri	2	0	4	6	364.4	17.7	113	DV UMa	1	0	3	3	429.8	18.6	277
AQ Eri	4	0	10	6	412.4	17.7		DW UMa	7	0	10	8	547.6	14.9	
AW Gem	4	0	9	6	451.6	18.8		UX UMa	7	0	14	12	612.8	12.7	250
CE Gru	5	0	6	3	367.0	18.0		RW UMi	9	0	5	5	1321.0	18.8	
DQ Her	6	0	13	9	1271.2	14.2	330	PW Vul	9	0	2	3	597.8		
V533 Her	9	0	6	6	1084.0	14.3		H1929+509	0	1	6	2	1008.8	17.3	
WW Hor	5	1	11	9	550.8	18.8	430								

[a] observed in period 5-10 August 1991

In order to check for irregularities in the automatic detections procedures, we made contour plots of the background-subtracted image. This may reveal contamination of the region close to the cataclysmic variable by another bright source, which would lead to an erroneously large claimed detection. It also may show the occasional misplacement of source photons along the direction of the scan, which would lead to an underestimated countrate (see Belloni et al. 1994). Neither irregularity was encountered.

Because the sensitivity of the PSPC detector is highest in the center, and less in the perifery, the effective exposure time is less than the geometric exposure time during which a source is in the field of view during the scans. One may correct for this either by correcting exposure time to the value corresponding to on-axis sensitivity, the effective exposure time; or by correcting the number of detected counts to the number which would have been detected if the source had been on-axis during the geometric exposure time, i.e. making a vignetting correction. In Table 1 we list for the detected cataclysmic variables the actual number of counts detected in the total band, and the effective exposure time. The total countrate is given by the ratio of these two numbers. We also give the actual number of detected counts in the separate bands, i.e. not corrected for vignetting.

In Table 2 we list the cataclysmic variables that were not detected, with the upper limits to the number of counts detected in the total bandpass and in bandpass B, not corrected for vignetting, as well as the effective exposure time.

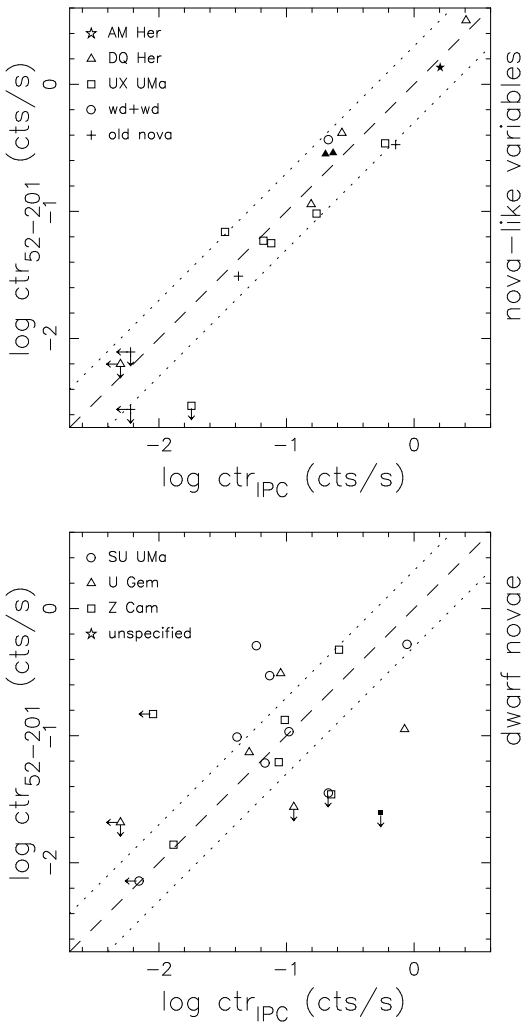

Fig. 2. Comparison between the countrates as observed with the Einstein IPC and with the ROSAT PSPC, for nova-like variables (top panel) and dwarf novae (lower panel). A filled symbol indicates an X-ray selected system, i.e. a system first discovered in X-rays, and subsequently identified with a previously unknown cataclysmic variable. Upper limits are marked with arrows. The dashed line indicates equal countrates in IPC and PSPC (channels 52-201), the dotted lines a difference in countrates of a factor 2.

3. Results

3.1. Comparison with Einstein IPC results

As a first inspection of our results, we compare the countrates detected in the ROSAT Survey with those found in pointed observations with the Einstein IPC. The Einstein IPC is not very sensitive to photons with energies less than 0.5 keV, whereas the ROSAT countrate for such photons is strongly affected by interstellar absorption. For this reason we plot the countrates detected in channels 52-201 as a function of the IPC countrate in Fig. 2. The Einstein IPC countrates were taken mainly from Eracleous et al. (1991); for sources not listed there, the countrates were taken from Córdova & Mason (1984). The countrate of EF Eri is from Patterson et al. (1981). We always use the longest reported observation. For the nova-like variables the ROSAT countrates are well correlated with the Einstein countrates. Fortuitously, the countrates are virtually the same in both instruments. The energy-dependence of the sensitivity of the Einstein IPC is different from that of the ROSAT PSPC, and thus it is possible, in principle, that a peculiar X-ray spectrum (e.g. with strong lines) would have a very different effect in one detector than in the other. The good correlation indicates that no such peculiarities are present.

All nova-like variables detected by Einstein and investigated for this article were detected during the ROSAT Survey, with one exception, viz. V Sge, which was not detected with ROSAT. The high quality of the mirrors of the ROSAT X-ray telescope causes only a very low background in the PSPC detector, and thus sources can be detected in exposures during the survey which are more than an order of magnitude shorter than those of the pointed Einstein observations.

For dwarf novae there appears little correlation between the two countrates. In view of the good correlation for the nova-like variables, it may well be that the differences for dwarf novae reflect real differences in X-ray flux. Such differences can arise because of the variability in X-ray flux between outburst and quiescence. We have therefore used the AAVSO Circulars (Bortle 1979, 1980, 1990, 1991) to investigate the outburst status during both the Einstein and the ROSAT All Sky Survey observations. If the Einstein or ROSAT observation occurs k days after the maximum of the previous outburst reported in the AAVSO Circulars, we denote this below as E k and R k. Quiescence, standstill and superoutburst are indicated with q, ss and so, respectively, and a question mark indicates that no optical information is available, which statistically may be expected to correspond to quiescence, since most systems spend rather more time in quiescence than in outburst. For the moment of the ROSAT observation we use the center, as given by Eq. 1, except for the systems flagged in Tables 1,2 with ^{a}, which were observed in August 1991. We use typical lightcurves of these systems to estimate the time required after outburst maximum to reach quiescence (see La Dous 1989).

We start by investigating the hypothesis that the X-ray countrate is lower during optical outburst from a moment somewhat after optical maximum until the optical flux has declined completely to the quiescent level (see Wheatley et al. 1996b), and that this explains the differences between ROSAT and Einstein countrates. The five dwarf novae well below the diagonal in Fig. 2 agree with the hypothesis, being in outburst when ROSAT observed, and (probably) in quiescence during the Einstein observation; V436 Cen (E 153, R so), BV Cen (E q, R ?), RX And (E 8, R ss), HL CMa (E ?, R 1), and RU Peg (E 45, R 7). For two dwarf novae well above the diagonal, SY Cnc (E 34, R 18) and WX Hyi (E 8, R 26), Córdova & Mason (1984) report outburst status during the Einstein observation, but the AAVSO Circulars do not report a maximum. The low Einstein flux of these two systems agrees with our hypothesis if they correspond to outburst. (From pointed ROSAT observations we know that WX Hyi is brighter in X-rays during quiescence – Van Teeseling and Verbunt 1994.) Two dwarf novae on the diagonal in

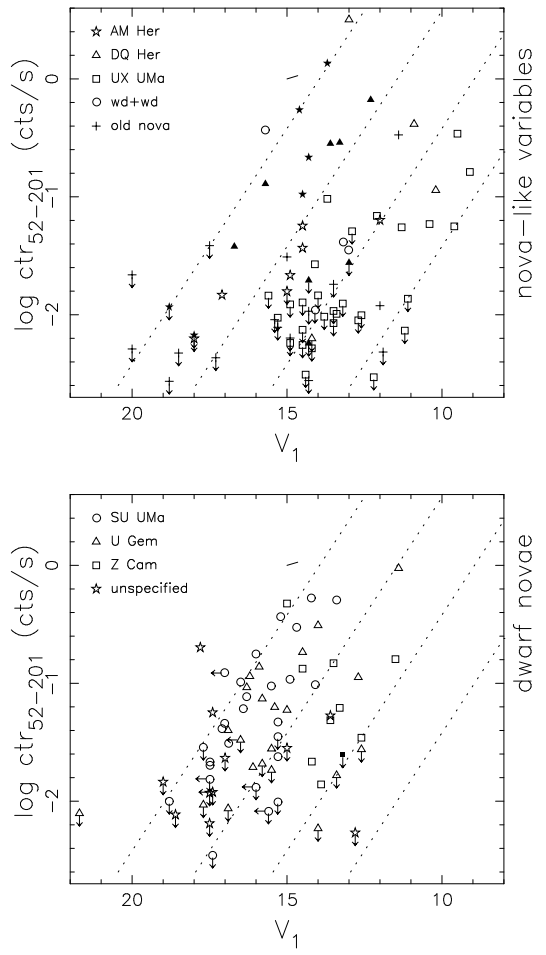

Fig. 3. Comparison between the countrates detected with the ROSAT PSPC and the flux in the visual. A filled symbol indicates an X-ray selected system. Upper limits are marked with arrows. For the visual magnitude V_1 we use the magnitude at which the system spends most of its time (listed as MAG1 in Ritter 1990). The dashed lines give constant ratios of the integrated X-ray flux to the integrated ultraviolet flux, calculated according to Eqs.2,3, i.e. for bremsstrahlung spectra and flat (f_ν =constant) optical ultraviolet spectra, for ratios 0.1, 0.01 and 0.001 and 0.0001. The short line starting at (15,0) shows the effect of interstellar absorption with $A_V = 0.11$ or $N_H = 2 \times 10^{20} cm^{-2}$.

Fig. 2 were in outburst during the Einstein observation and in quiescence when ROSAT observed: AH Her (E 0, R 13) and AB Dra (E 0, R 13). These agree with our hypothesis only if Einstein observed these systems at optical maximum, but before the X-ray flux dropped. The other dwarf novae close to the diagonal were in quiescence during both the Einstein and ROSAT observations.

So far, our hypothesis may have worked, but for the three remaining systems well above the diagonal in Fig. 2 our hypothesis certainly fails. VW Hyi (E 13, R 2) and YZ Cnc (E 11, R 1.5) were in quiescence during Einstein observations and in outburst during the ROSAT Survey, whereas U Gem (E 34, R >70) was in quiescence during both observations. ROSAT observed VW Hyi during a full outburst, but even though the PSPC countrate during outburst is lower than in quiescence, it is at all times much higher than the Einstein countrate (Wheatley et al. 1996b). The difference between the Einstein and ROSAT countrates of VW Hyi may be due to a long-term variation: Wheatley et al. suggest that this may be related to longer outburst intervals in 1990 than before. Whether a similar explanation holds for YZ Cnc and U Gem is not clear; it is also possible that these systems brighten in the ROSAT energy range during outburst.

3.2. Comparison with optical flux

In Fig. 3 we compare the countrate obtained during the ROSAT Survey with the visual flux. For the latter, we use the visual magnitude at which the cataclysmic variable is observed to spend most of its time, listed as MAG1 by Ritter (1990). For the X-ray countrate we again try to minimize the effect of interstellar absorption by taking the counts from channels 52-201. A thermal bremsstrahlung spectrum of 2 keV with an X-ray flux at Earth F produces a countrate in these channels given by

$$\log F_{0.01-10.0\mathrm{keV}}(\mathrm{ergcm^{-2}s^{-1}}) \simeq \log \mathrm{ctr}_{52-201}(\mathrm{s^{-1}}) - 10.54 \quad (2)$$

(as may be found by folding the spectrum with the PSPC sensitivity matrix). For an optical spectrum with f_ν =constant, the total optical and ultraviolet flux above the Lyman edge is related to the visual magnitude by

$$\log F_{90-900\mathrm{nm}}(\mathrm{ergcm^{-2}s^{-1}}) \simeq -0.4V - 3.96 \quad (3)$$

These two equations are used in Fig. 3 to indicate lines of constant X-ray to optical flux ratio.

In the diagram for the dwarf novae we note that the SU UMa systems and the U Gem systems on average have higher X-ray to optical flux ratios than the Z Cam systems. The highest flux ratio is for the little studied dwarf nova BZ UMa, followed by EK TrA. The high ratio for BZ UMa is probably due to an overestimate of its visual magnitude (at 17.8); Robertson & Honeycutt (1996) find $V \simeq 15.9$ for this system. The highest countrate is for SS Cyg. Comparison with the diagram for nova-like variables shows that the UX UMa systems have an even lower X-ray to optical flux ratio. We also note that for all of these systems the integrated X-ray flux is well below the integrated optical and ultraviolet flux. (Note that this does not include components of the X-ray spectrum too soft to be detected in the 0.5-2.5 keV band.) Virtually all nova-like variables with a X-ray to optical flux ratio higher than 0.01 are X-ray selected magnetic systems, i.e. AM Her or DQ Her type systems which were first discovered in X-rays. The three other systems with high flux ratios are the magnetic systems EX Hya and V1500 Cyg, and the double degenerate GP Com. The latter probably owes its exceptional position in the diagram to the low optical flux from its small accretion disk with low accretion rate. Comparison with the dwarf-nova diagram shows, however, that the X-ray flux of these sources in the 0.5-2.5 keV range is not higher than those of SU UMa and U Gem type systems with similar visual magnitudes.

A similar diagram may be made for the ultraviolet fluxes, albeit only for those fewer cataclysmic variables whose ultraviolet

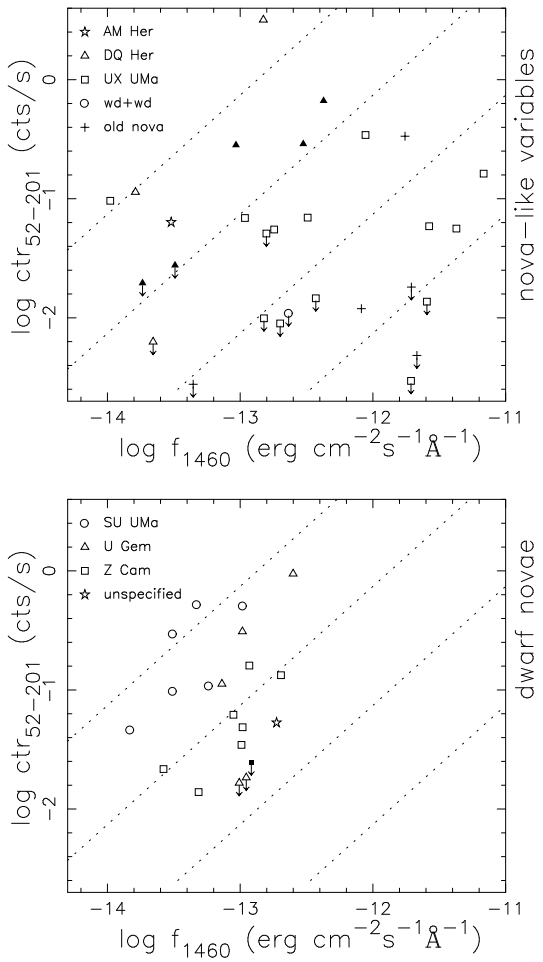

Fig. 4. Comparison between the countrates detected with the ROSAT PSPC and the flux in the ultraviolet, at λ = 1460Å, in units of erg $s^{-1}cm^{-2}Å^{-1}$. A filled symbol indicates an X-ray selected system. Upper limits are marked with arrows. The ultraviolet flux is corrected for absorption, and taken from Verbunt (1987) and from Appendix A. Dashed lines give flux ratios as in Fig. 3.

fluxes and reddenings are known (Verbunt 1987, and Appendix A). This diagram, shown in Fig. 4, shows much the same structure as that with the optical magnitudes. The ultraviolet flux is a cleaner measure of the accretion process near the white dwarf than the optical flux, because it is less affected by the size of the accretion disk and by contributions from the companion star. GK Per and V794 Aql do not have a high X-ray to optical flux ratio, but are amongst the three systems with the highest X-ray to ultraviolet flux ratios. For AM Her we selected ultraviolet observations obtained in its low state, as this system was in its low state during the ROSAT All Sky Survey; in Fig. 4 the system now shows up with a high X-ray to ultraviolet flux ratio, in its low state.

The ratio of X-ray count rate to ultraviolet flux is of interest for the identification of X-ray sources in the cores of globular clusters, as cataclysmic variables stand out more at ultraviolet wavelengths. Fig. 4 suggests that a preliminary classification can be made of sources based on the ratio of the ROSAT countrate to the ultraviolet flux.

3.3. X-ray colours

A first idea of the X-ray spectral flux distribution may be obtained by inspecting the distribution of detected counts over the energy channels. In Fig. 5 we show the count ratios between the soft (channels 11-41) and hard (channels 52-201) bands, as well as the ratio between two bands in the hard range (channels 52-90 and 91-201). In each graph, only those points are shown which are detected with errors less than 30% in the countrates of both bands.

The count ratio of channels 52-90 and 92-201 is seen to lie in a fairly narrow range. The width of this range in fact is compatible with being due to errors in the countrate. Thus, within these bands there is no evidence for widely varying flux distributions. This remains true if we take the upper limits – not shown in the figure – into account.

The count ratio of channels 11-41 and 52-201 has a wider range. At the soft end, this is due to the detection in channels 11-41 of the very soft components in the spectra of AM Her type systems. Several of these systems, including the systems DP Leo and EK UMa, which were not detected in the hard bands, have a countrate in the soft band more than an order of magnitude higher than in the hard band. The dwarf nova SS Cyg is also remarkably soft; this is due to the fact that this system was in outburst during the All Sky Survey, showing enhanced soft X-ray emission (as described in detail by Ponman et al. 1995). At the hard end, the range of count ratios is wider than shown in Fig. 5, due to systems not detected in the soft band. Part of this is due to the effect of interstellar absorption: for example, the count ratio of channels 11-41 and 52-201 for a 2 keV bremsstrahlung spectrum is reduced from 1.6 at zero absorption to 0.4 when absorbed by an interstellar column of $N_H = 2 \times 10^{20} \mathrm{cm}^{-2}$ (corresponding very roughly to optical reddening of $E(B-V) = 0.036$; see Predehl & Schmitt 1995).

3.4. X-ray luminosities

To transform the observed ROSAT PSPC countrates to an X-ray luminosity requires knowledge of the X-ray spectrum and of the distance. The countrate in the lower energy channels are strongly affected by interstellar absorption, and we therefore use only the counts in channels 52-201 when transforming observed countrates into luminosity. The X-ray luminosity that we will quote will be that in the range between 0.5-2.5 keV. This choice takes account of the lack of information on the spectrum outside the ROSAT bandpass, and minimizes the possible errors in the transformation of countrate to flux. For the distances we use the values listed in Tables 1,2.

For a 2 keV bremsstrahlung spectrum, not affected by absorption, a PSPC countrate ctr_{52-201} in channels 52-201 corresponds to a flux in the 0.5-2.5 keV range given by

$$\log F_{0.5-2.5\mathrm{keV}}(\mathrm{ergcm}^{-2}\mathrm{s}^{-1}) \simeq \log \mathrm{ctr}_{52-201}(\mathrm{s}^{-1}) - 10.88 \quad (4)$$

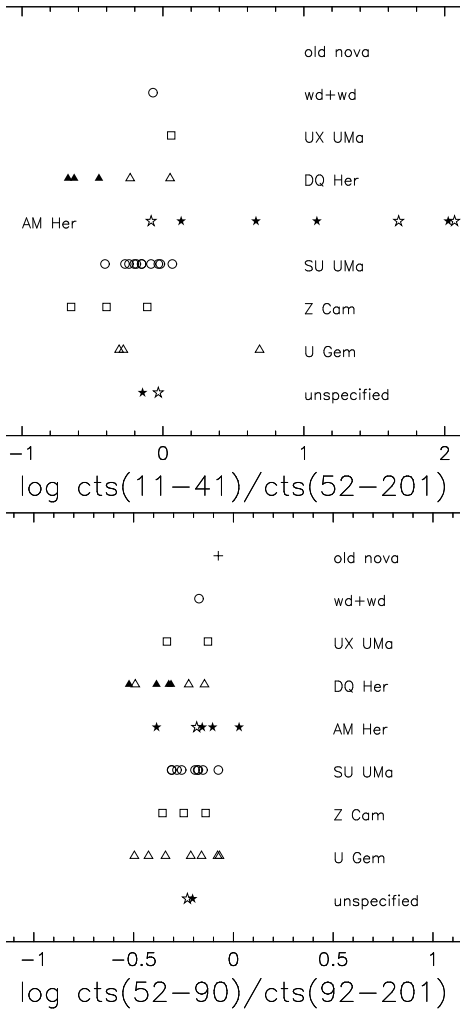

Fig. 5. ROSAT PSPC count ratios obtained during the All Sky Survey; in each graph only those systems are included for which the error in both countrates is less than 30%. Hard (soft) spectra are on the left (right) in these diagrams. Filled symbols denote X-ray selected systems.

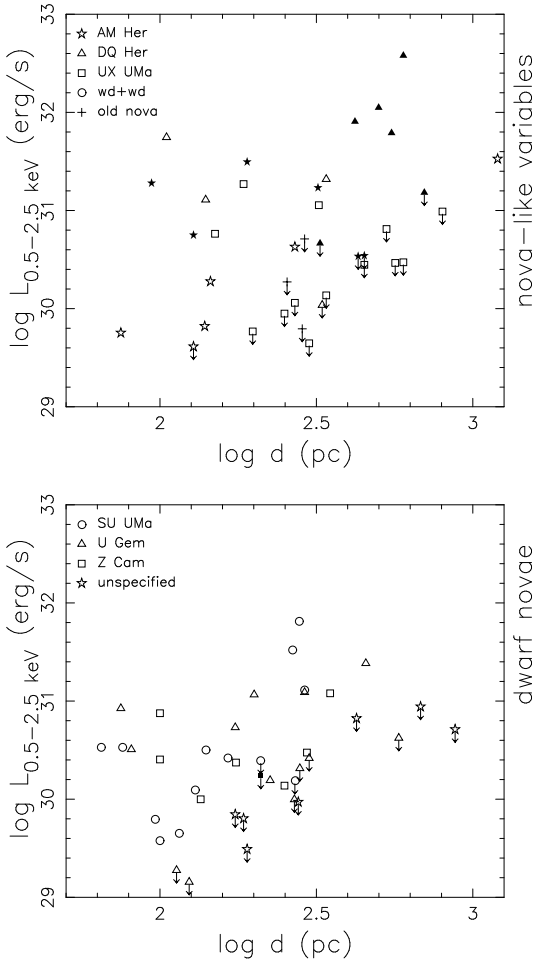

Fig. 6. Luminosities in the 0.5-2.5 keV range as a function of distance, calculated using Eq.4. No corrections for interstellar absorption have been applied. A filled symbol indicates an X-ray selected system. Upper limits are marked with arrows.

In Fig. 6 we show the luminosity distributions derived from the ROSAT PSPC All Sky Survey.

The range of luminosities is wide, four orders of magnitude. This implies that errors in the distances, even up to a factor 2, will not much affect the general structure of Fig. 6. The brightest nova-like variables are all DQ Her systems, most of them X-ray selected, i.e. first discovered in X-rays and subsequently identified with a previously unknown cataclysmic variable. All of these are at relatively large distances, suggesting that such X-ray luminous cataclysmic variables are relatively rare. The brightest system is V1223 Sgr. In the 0.5-2.5 keV range, the AM Her systems are not more luminous than other cataclysmic variables.

Regarding the dwarf novae, it is striking that the best studied systems, SS Cyg, U Gem and VW Hyi are bright because of their proximity to Earth, rather than intrinsically luminous. The three most luminous dwarf novae are SU UMa, WX Hyi and TW Vir. The least luminous system in our sample (not shown in the figure) is AY Lyr, only marginally detected at $L_{0.5-2.5keV} \sim 3 \times 10^{28}$ erg/s, notwithstanding its proximity.

The X-ray luminosity distributions of the different classes of cataclysmic variables are indistinguishable, with the exception of the (mainly X-ray selected) DQ Her type systems, which range to higher luminosities than the other types. The X-ray luminosities of the double degenerate systems, such as GP Com and AM CVn, are not known as the distances to these systems are not known.

4. Discussion

Out of the 162 cataclysmic variables with known or suspected orbital periods, we have detected 91 systems. Ordering the detections on total countrate, we find that 7 of the 10 brightest systems are AM Her type systems, the other three being the nearby dwarf novae VW Hyi and SS Cyg, and the DQ Her system EX Hya. The same ten systems, in slightly different order,

are also the ten brightest systems at soft energies, 0.1-0.5 keV. Amongst the ten systems with the highest countrates at energies $0.5 - 2.5$ keV, only two are AM Her type systems, confirming the known fact that these systems emit the bulk of their luminosity as soft X-rays. The well-studied system AM Her was in a low state during the ROSAT Survey.

For nova-like variables, the countrates obtained with ROSAT correlate very well with those found with the Einstein IPC. The dwarf novae countrates are less well correlated, as some systems were observed in outburst with ROSAT and in quiescence with the Einstein IPC or vice versa. Two systems however, (VW Hyi and U Gem) were found to be much brighter in the ROSAT Survey than during the Einstein observation, even though they were in the same outburst state. We can offer no explanation for this other than assuming that these systems show long-term variation in their X-ray flux (see also Wheatley et al. 1996b).

When plotting the 0.5-2.5 keV countrate as a function of visual flux, we find that the different classes of cataclysmic variables are roughly separated. (This is also true for the 0.1-2.5 keV countrate, see Verbunt 1996b.) Generally speaking the ratio of X-ray to optical flux decreases along the sequence SU UMa, U Gem, Z Cam and UX UMa types. It has been suggested that this sequence is one of increasing accretion rate, in which case our finding is in general agreement with the result by Patterson & Raymond (1985) that high accretion rate corresponds to low X-ray to optical flux ratio, for non-magnetic systems. It should be noted that this general pattern is perturbed by the anticorrelation of the inclination of the cataclysmic variable orbit and the X-ray luminosity observed on Earth (Van Teeseling et al. 1996). In Fig. 3 the visual magnitude shown is that of the system in quiescence. The optical flux of dwarf novae increases dramatically during an outburst, whereas the 0.5-2.5 keV flux of most of these systems appears to be suppressed; dwarf novae that were in outburst during the ROSAT Survey observations are therefore shown at too low an X-ray to optical flux ratio in this figure. X-ray luminosities of 37 cataclysmic variables have also been determined from PSPC data of ROSAT pointed observations by Richman (1996); their values are conform to the above picture.

Many of the (AM Her and DQ Her) magnetic systems are X-ray selected, i.e. they were discovered as X-ray sources and subsequently identified with previously unknown cataclysmic variables. These discoveries often were made at energies above 2 keV. It is therefore remarkable to see in Fig. 3 that the $0.5 - 2.5$ keV X-ray to optical flux ratio for magnetic systems is not higher than that of the SU UMa systems. Optical identification of X-ray sources from the ROSAT All Sky Survey leads to the discovery of new X-ray selected cataclysmic variable systems; From Tables 5 and 6 of Motch et al. (1996; note $\mathrm{ctr}_{52-201} \simeq 0.5[\mathrm{HR1} + 1] \times \mathrm{ctr}_{11-201}$), we find that they have similar X-ray to optical flux ratios as the X-ray selected systems known before the ROSAT mission, as shown in Fig. 7. The exception is RXJ1914.4+2456, a heavily absorbed very soft source (Haberl & Motch 1995), and a member of a new class of cataclysmic variables, with magnetic fields like the DQ Her systems, but

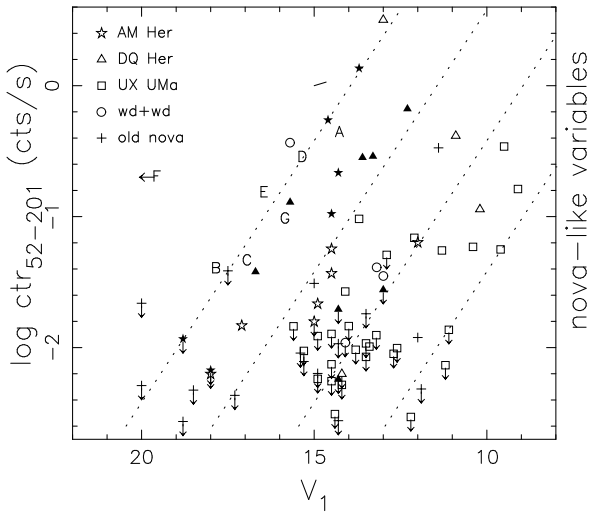

Fig. 7. Location of newly identified cataclysmic variables from the ROSAT All Sky Survey (Motch et al. 1996), indicated with roman capital letters, in the X-ray to optical flux ratio diagram. F is RXJ1914.4+2456, a heavily absorbed ($A_V \sim 5.6$) ultrasoft source.

with a strong very soft component in their X-ray spectrum. This new class will extend the range of DQ Her type systems in the $\log(\mathrm{ctr}_{11-40}/\mathrm{ctr}_{52-201})$ diagram of Fig. 5 to the soft end.

Figs. 3 and 4 may also be of use in determining whether some of the low-luminosity X-ray sources discovered in globular clusters are cataclysmic variables, as is discussed in Appendix B (see also Johnston & Verbunt 1996).

The $0.5 - 2.5$ keV luminosity distributions of the different type of cataclysmic variables is rather similar, ranging up to $\sim 10^{32}$erg/s (Fig. 6). This implies that most of the variation in X-ray to optical flux ratio is due to variations in the optical flux, as has been pointed out before on the basis of pointed ROSAT observations (van Teeseling & Verbunt 1994, van Teeseling et al. 1996). The spectral flux distribution within the 0.5-2.5 bandpass appears to be fairly similar for most systems (Fig. 5), which implies that the conversion of countrate to flux is accurate, even for AM Her type systems. The example of RXJ1914.4+2456 gives a warning that the conversion may go badly wrong for heavily absorbed systems, whose very soft spectra do not contain a detected hard component.

Acknowledgements. The ROSAT project is supported by the Bundesministerium für Forschung und Technologie (BMFT) and by the Max Planck Gesellschaft. FV is supported by NWO under grant PGS 78-277.

Appendix A: additional ultraviolet data

The overview by Verbunt (1987) of ultraviolet observations of cataclysmic variables obtained with the *International Ultraviolet Explorer* is limited to non-magnetic systems whose orbital periods were known at the time. We have investigated the archive of *IUE* low-resolution spectra for additional information. To determine the reddening of a cataclysmic variable, we require a

Table 3. Reddenings and fluxes of cataclysmic variables and the *IUE* spectra from which they are determined. For dwarf novae we also list the spectra obtained in quiescence from which we determine the fluxes used in Fig. 4. With f_λ the flux in 10^{-13} erg cm^{-2}s^{-1}Å^{-1}, the Table lists log $f_{1460\text{Å}}$, log($f_{1460\text{Å}}/f_{1800\text{Å}}$) and log($f_{1460\text{Å}}/f_{2880\text{Å}}$).

name	SWP	LWR	$E(B-V)$	1460	$\frac{1460}{1800}$	$\frac{1460}{2880}$
AM CVn	19546	15583	<0.03	0.365	0.221	0.681
AM Her	21437	2207[1]	0.00	−.520	0.325	0.575
V426 Oph	8069	7036	<0.10			
	28946	8941[1]		0.069	0.125	0.447
V442 Oph	15259	11773	0.20±0.05	0.570	0.206	0.559
V841 Oph	7950	6925	0.50±0.10	1.290	0.243	0.792
GK Per	20653	16563	0.20±0.05			
	15311	11849		−.789	−.091	−.176
VY Scl	6123	5303	<0.05	0.197	0.158	0.432
UZ Ser	17633	13901	0.30±0.05			
	17700	13960		0.046	0.322	0.902

[1]LWP spectrum

high quality spectrum obtained with the *IUE* LWR camera, and a quasi-simultaneous short wavelength spectrum. Most systems in our sample that were not discussed by Verbunt (1987) are either too faint ($V \gtrsim 15$) for good quality *IUE* spectra, or have been observed with the LWP camera, which provides very noisy data in the 2000-2400Å range.

Table 3 lists the systems that we were able to add, and the reddenings that we determined for them. For nova-like variables the reddening was determined from the same spectra as gave the fluxes at 1460Å, but for dwarf novae the reddening is determined from outburst spectra, whereas the fluxes used in Fig. 4 were obtained from spectra of the quiescent dwarf nova. We give fluxes for AM Her in its low state (Heise & Verbunt 1987). In this paper we also use the revised reddening to RR Pic determined by van Teeseling et al. (1996). Fluxes are determined in 80Å wide bands, centered on 1460, 1800, and 2880Å, as described in Verbunt (1987).

Appendix B: cataclysmic variables in globular clusters

Figs. 3 and 4 may be used to determine whether an optically identified X-ray source is likely to be a cataclysmic variable. If the distance to the source is known, the information provided by the absolute magnitude and the X-ray luminosity can also be used. Such is the case for example for the low-luminosity X-ray sources in globular clusters, which have been suggested to be cataclysmic variables, but for which other identifications have also been suggested, viz. RS CVn binaries, recycled (or millisecond) radio pulsars, and soft X-ray transients in quiescence. This assumes that cataclysmic variables in globular clusters have properties similar to those in the galactic disk, which need not be the case, as the formation mechanisms may be very different in clusters and in the disk (Bailyn 1995).

In Fig. 8 we compare the X-ray luminosities of the cataclysmic variables as observed in the ROSAT All Sky Survey with those of RS CVn systems (values from Dempsey et al. 1993, multiplied by 0.4 to correct for the different energy range),

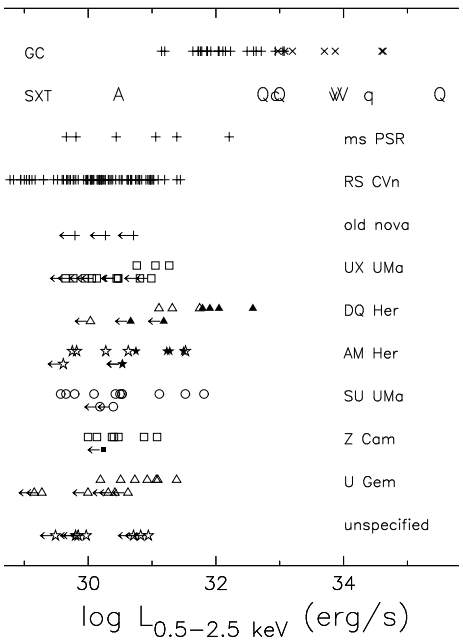

Fig. 8. 0.5-2.5 keV X-ray luminosities of various classes of cataclysmic variables, compared with those of RS CVn's, recycled radio pulsars, soft X-ray transients in quiescence, and sources in the cores of globular clusters. For each class of cataclysmic variables, the upper limits are shown below the detections. For the soft X-ray transients, lower case indicates *Einstein* detections, upper case ROSAT detections; A = A 0620 − 00, Q = Aql X-1, c = Cen X-4, V = V404 Cyg. For the cluster sources + and × indicate luminosities based on a known, or assumed, spectrum, respectively.

recycled radio pulsars (values from Becker & Trümper 1997, multiplied by 0.29 to correct for the different energy range), soft X-ray transients (from Verbunt 1996a), and the low-luminosity sources in the cores of globular clusters (from Johnston & Verbunt 1996). Fig. 8 confirms the statements made first by Verbunt et al. (1984) that the brightest low-luminosity X-ray sources in the cores of globular clustes are too bright to be cataclysmic variables, and that their luminosities are compatible with those of soft X-ray transients in quiescence. The figure also confirms the statement by Cool et al. (1995) that the X-ray sources in NGC 6397, with $L_x(0.5-2.5) \simeq 5 \times 10^{31}$erg/s, could be cataclysmic variables. The three cataclysmic variables with the highest X-ray luminosities in Fig. 8 are the X-ray DQ Her type systems V1223 Sgr, AO Psc and TV Col, all three X-ray selected systems, with absolute visual magnitudes (corrected also for reddening) M_V = 2.9, 4.9 and 5.1, respectively (V from Ritter 1990, $E(B-V)$ from Verbunt 1987, distance from Table 1). The proposed optical counterparts for the dim X-ray sources in NGC 6397 have absolute (red) magnitudes ranging from 5.6 to 7.3; the absolute visual magnitudes will be similar (see the spectra in Grindlay et al. 1995). The brightest of these is therefore similar to AO Psc, and the optically fainter one to EX Hya, which has $M_V \simeq 7.9$.

The suggestion by Danner et al. (1994) that rapidly rotating recycled pulsars are possible counterparts for dim X-ray sources in globular clusters is also borne out by Fig. 8; the brightest pulsar in that figure being PSR J0218+4232 (Verbunt et al. 1996).

References

Bailyn, C. 1995, ARA&A, 33, 133
Becker, W., Trümper, J. 1997, A&A, in press
Belloni, T., Hasinger, G., Izzo, C. 1994, A&A, 283, 1037
Beuermann, K., Thomas, H.-C. 1993, Adv. Space Res., 13(12), 115
Bortle, J. 1979, AAVSO Circular, 99-110
Bortle, J. 1980, AAVSO Circular, 111-120
Bortle, J. 1990, AAVSO Circular, 238-242
Bortle, J. 1991, AAVSO Circular, 243
Cool, A., Grindlay, J., Cohn, H., Lugger, P., Slavin, S. 1995, ApJ, 439, 695
Córdova, F. 1995, in W. Lewin, J. van Paradijs, E. van den Heuvel (eds.), X-ray Binaries, Cambridge University Press, p. 331
Córdova, F., Mason, K. 1983, in W. Lewin, E. van den Heuvel (eds.), Accretion-driven stellar X-ray sources, Cambridge University Press, p. 147
Córdova, F., Mason, K. 1984, MNRAS, 206, 879
Cruddace, R., Hasinger, G., Schmitt, J. 1988, in F. Murtagh, A. Heck (eds.), Astronomy from large databases, p. 177
Danner, R., Kulkarni, S., Thorsett, S. 1994, ApJ (Letters), 436, L153
Dempsey, R., Linsky, J., Fleming, T., Schmitt, J. 1993, ApJS, 86, 599
Eracleous, M., Halpern, J., Patterson, J. 1991, ApJ, 382, 290
Forman, W., Jones, C., Cominsky, L., Julien, P., Murray, S., Peters, G., Tananbaum, H., Giacconi, R. 1978, ApJS, 38, 357
Grindlay, J., Cool, A., Callanan, P., Bailyn, C., Cohn, H., Lugger, P. 1995, ApJ, 455, L47
Haberl, F., Motch, C. 1995, A&A, 297, L37
Heise, J., Verbunt, F. 1987, A&A, 189, 112
Heise, J., Mewe, R., Brinkman, A. et al., 1978, A&A, 63, L1
Johnston, H., Verbunt, F. 1996, A&A, 312, 80
Kraft, R. 1990, in A. Casatella, R. Viotti (eds.), Physics of classical novae, IAU Coll.122, Springer Verlag, Berlin, p. 3
La Dous, C. 1989, IUE-ULDA Access Guide No.1 Dwarf Novae and Nova-like Stars, ESA SP 1114, Noordwijk
Mauche, C. 1997, in F. Makino, K. Mitsuda (eds.), X-ray imaging and spectroscopy of cosmic hot plasmas, Universal Academy Press, Tokyo, p. 529
Motch, C., Haberl, F., Guillout, P., Pakull, M., Reinsch, K., Krautter, J. 1996, A&A, 307, 459
Patterson, J., Raymond, J. 1985, ApJ, 292, 535
Patterson, J., William, G., Hiltner, W. 1981, ApJ, 245, 618
Pfeffermann, E., Briel, U., Hippmann, H. et al., 1986, SPIE — Soft X-ray Optics and Technology, 733, 519
Ponman, T., Belloni, T., Duck, S., Verbunt, F., Watson, M., Wheatley, P., Pfeffermann, E. 1995, MNRAS, 276, 495
Predehl, P., Schmitt, J. 1995, A&A, 293, 889
Rappaport, S., Cash, W., Doxsey, R., McClintock, J., Moore, G. 1974, ApJ (Letters), 187, L5
Reimers, D., Griffin, R., Brown, A. 1988, A&A, 193, 180
Richman, H. 1996, ApJ, 462, 404
Ritter, H. 1990, A&AS, 85, 1179
Ritter, H., Kolb, U. 1995, in W. Lewin, J. van Paradijs, E. van den Heuvel (eds.), X-ray Binaries, Cambridge University Press, p. 578
Robertson, J., Honeycutt, R. 1996, AJ, 112, 2248
Rutten, R., van Paradijs, J., Tinbergen, J. 1992, A&A, 260, 213
Sproats, L., Howell, S., Mason, K. 1996, MNRAS, 282, 1211
van Teeseling, A., Beuermann, K., Verbunt, F. 1996, A&A, 315, 467
van Teeseling, A., Verbunt, F. 1994, A&A, 292, 519
Verbunt, F. 1987, A&AS, 71, 339
Verbunt, F. 1996a, in J. van Paradijs, E.P.J. van den Heuvel, E. Kuulkers (eds.), Compact stars in binaries, IAU Symp. 165, Kluwer Academic Publishers, Dordrecht, p. 333
Verbunt, F. 1996b, in H. Zimmermann, J. Trümper, H. Yorke (eds.), Roentgenstrahlung from the Universe, MPE Report 263, p. 93
Verbunt, F., Bunk, W., Hasinger, G., Johnston, H. 1995, A&A, 300, 732
Verbunt, F., Kuiper, L., Belloni, T. et al., 1996, A&A, 311, L9
Verbunt, F., van Paradijs, J., Elson, E. 1984, MNRAS, 210, 899
Voges, W. 1992, in Proceedings of European ISY meeting: Space Science with particular emphasis on High Energy Astrophysics, ESA SP-349, p. 300
Warner, B. 1976, in P. Eggleton, S. Mitton, J. Whelan (eds.), The Structure and Evolution of Close Binary Systems, IAU Symposium 73, Reidel, Dordrecht, p. 85
Warner, B. 1987, MNRAS, 227, 23
Warner, B. 1995, Cataclysmic variables, Cambridge University Press
Wheatley, P., van Teeseling, A., Watson, M., Verbunt, F., Pfeffermann, E. 1996a, MNRAS, 283, 101
Wheatley, P., Verbunt, F., Belloni, T., Watson, M., Naylor, T., Ishida, M., Duck, S., Pfeffermann, E. 1996b, A&A, 307, 137
Zimmermann, H., Belloni, T., Izzo, C., Kahabka, P., Schwentker, O. 1992, EXSAS User's Guide: Extended scientific analysis system to evaluate data from the astronomical X-ray satellite ROSAT, Technical Report 48, MPE

This article was processed by the author using Springer-Verlag LaTeX A&A style file *L-AA* version 3.